EUROPEAN ORGANIZATION FOR NUCLEAR RESEARCH (CERN)

CERN-PH-EP-2013-062
LHCb-PAPER-2013-014
June 24, 2013

arXiv:1304.4518v2 [hep-ex] 21 Jun 2013

Searches for violation of lepton flavour and baryon number in tau lepton decays at LHCb

The LHCb collaboration[†]

Abstract

Searches for the lepton flavour violating decay $\tau^- \to \mu^-\mu^+\mu^-$ and the lepton flavour and baryon number violating decays $\tau^- \to \bar{p}\mu^+\mu^-$ and $\tau^- \to p\mu^-\mu^-$ have been carried out using proton-proton collision data, corresponding to an integrated luminosity of 1.0 fb^{-1}, taken by the LHCb experiment at $\sqrt{s} = 7\,\text{TeV}$. No evidence has been found for any signal, and limits have been set at 90% confidence level on the branching fractions: $\mathcal{B}(\tau^- \to \mu^-\mu^+\mu^-) < 8.0 \times 10^{-8}$, $\mathcal{B}(\tau^- \to \bar{p}\mu^+\mu^-) < 3.3 \times 10^{-7}$ and $\mathcal{B}(\tau^- \to p\mu^-\mu^-) < 4.4 \times 10^{-7}$. The results for the $\tau^- \to \bar{p}\mu^+\mu^-$ and $\tau^- \to p\mu^-\mu^-$ decay modes represent the first direct experimental limits on these channels.

Submitted to Physics Letters B

© CERN on behalf of the LHCb collaboration, license CC-BY-3.0.

[†]Authors are listed on the following pages.

LHCb collaboration

R. Aaij[40], C. Abellan Beteta[35,n], B. Adeva[36], M. Adinolfi[45], C. Adrover[6], A. Affolder[51], Z. Ajaltouni[5], J. Albrecht[9], F. Alessio[37], M. Alexander[50], S. Ali[40], G. Alkhazov[29], P. Alvarez Cartelle[36], A.A. Alves Jr[24,37], S. Amato[2], S. Amerio[21], Y. Amhis[7], L. Anderlini[17,f], J. Anderson[39], R. Andreassen[56], R.B. Appleby[53], O. Aquines Gutierrez[10], F. Archilli[18], A. Artamonov [34], M. Artuso[57], E. Aslanides[6], G. Auriemma[24,m], S. Bachmann[11], J.J. Back[47], C. Baesso[58], V. Balagura[30], W. Baldini[16], R.J. Barlow[53], C. Barschel[37], S. Barsuk[7], W. Barter[46], Th. Bauer[40], A. Bay[38], J. Beddow[50], F. Bedeschi[22], I. Bediaga[1], S. Belogurov[30], K. Belous[34], I. Belyaev[30], E. Ben-Haim[8], G. Bencivenni[18], S. Benson[49], J. Benton[45], A. Berezhnoy[31], R. Bernet[39], M.-O. Bettler[46], M. van Beuzekom[40], A. Bien[11], S. Bifani[44], T. Bird[53], A. Bizzeti[17,h], P.M. Bjørnstad[53], T. Blake[37], F. Blanc[38], J. Blouw[11], S. Blusk[57], V. Bocci[24], A. Bondar[33], N. Bondar[29], W. Bonivento[15], S. Borghi[53], A. Borgia[57], T.J.V. Bowcock[51], E. Bowen[39], C. Bozzi[16], T. Brambach[9], J. van den Brand[41], J. Bressieux[38], D. Brett[53], M. Britsch[10], T. Britton[57], N.H. Brook[45], H. Brown[51], I. Burducea[28], A. Bursche[39], G. Busetto[21,q], J. Buytaert[37], S. Cadeddu[15], O. Callot[7], M. Calvi[20,j], M. Calvo Gomez[35,n], A. Camboni[35], P. Campana[18,37], D. Campora Perez[37], A. Carbone[14,c], G. Carboni[23,k], R. Cardinale[19,i], A. Cardini[15], H. Carranza-Mejia[49], L. Carson[52], K. Carvalho Akiba[2], G. Casse[51], L. Castillo Garcia[37], M. Cattaneo[37], Ch. Cauet[9], M. Charles[54], Ph. Charpentier[37], P. Chen[3,38], N. Chiapolini[39], M. Chrzaszcz [25], K. Ciba[37], X. Cid Vidal[37], G. Ciezarek[52], P.E.L. Clarke[49], M. Clemencic[37], H.V. Cliff[46], J. Closier[37], C. Coca[28], V. Coco[40], J. Cogan[6], E. Cogneras[5], P. Collins[37], A. Comerma-Montells[35], A. Contu[15,37], A. Cook[45], M. Coombes[45], S. Coquereau[8], G. Corti[37], B. Couturier[37], G.A. Cowan[49], D.C. Craik[47], S. Cunliffe[52], R. Currie[49], C. D'Ambrosio[37], P. David[8], P.N.Y. David[40], A. Davis[56], I. De Bonis[4], K. De Bruyn[40], S. De Capua[53], M. De Cian[39], J.M. De Miranda[1], L. De Paula[2], W. De Silva[56], P. De Simone[18], D. Decamp[4], M. Deckenhoff[9], L. Del Buono[8], N. Déléage[4], D. Derkach[14], O. Deschamps[5], F. Dettori[41], A. Di Canto[11], F. Di Ruscio[23,k], H. Dijkstra[37], M. Dogaru[28], S. Donleavy[51], F. Dordei[11], A. Dosil Suárez[36], D. Dossett[47], A. Dovbnya[42], F. Dupertuis[38], R. Dzhelyadin[34], A. Dziurda[25], A. Dzyuba[29], S. Easo[48,37], U. Egede[52], V. Egorychev[30], S. Eidelman[33], D. van Eijk[40], S. Eisenhardt[49], U. Eitschberger[9], R. Ekelhof[9], L. Eklund[50,37], I. El Rifai[5], Ch. Elsasser[39], D. Elsby[44], A. Falabella[14,e], C. Färber[11], G. Fardell[49], C. Farinelli[40], S. Farry[12], V. Fave[38], D. Ferguson[49], V. Fernandez Albor[36], F. Ferreira Rodrigues[1], M. Ferro-Luzzi[37], S. Filippov[32], M. Fiore[16], C. Fitzpatrick[37], M. Fontana[10], F. Fontanelli[19,i], R. Forty[37], O. Francisco[2], M. Frank[37], C. Frei[37], M. Frosini[17,f], S. Furcas[20], E. Furfaro[23,k], A. Gallas Torreira[36], D. Galli[14,c], M. Gandelman[2], P. Gandini[57], Y. Gao[3], J. Garofoli[57], P. Garosi[53], J. Garra Tico[46], L. Garrido[35], C. Gaspar[37], R. Gauld[54], E. Gersabeck[11], M. Gersabeck[53], T. Gershon[47,37], Ph. Ghez[4], V. Gibson[46], V.V. Gligorov[37], C. Göbel[58], D. Golubkov[30], A. Golutvin[52,30,37], A. Gomes[2], H. Gordon[54], M. Grabalosa Gándara[5], R. Graciani Diaz[35], L.A. Granado Cardoso[37], E. Graugés[35], G. Graziani[17], A. Grecu[28], E. Greening[54], S. Gregson[46], P. Griffith[44], O. Grünberg[59], B. Gui[57], E. Gushchin[32], Yu. Guz[34,37], T. Gys[37], C. Hadjivasiliou[57], G. Haefeli[38], C. Haen[37], S.C. Haines[46], S. Hall[52], T. Hampson[45], S. Hansmann-Menzemer[11], N. Harnew[54], S.T. Harnew[45], J. Harrison[53], T. Hartmann[59], J. He[37], V. Heijne[40], K. Hennessy[51], P. Henrard[5], J.A. Hernando Morata[36], E. van Herwijnen[37], E. Hicks[51], D. Hill[54], M. Hoballah[5], C. Hombach[53], P. Hopchev[4], W. Hulsbergen[40], P. Hunt[54], T. Huse[51], N. Hussain[54], D. Hutchcroft[51], D. Hynds[50], V. Iakovenko[43], M. Idzik[26], P. Ilten[12], R. Jacobsson[37], A. Jaeger[11], E. Jans[40], P. Jaton[38],

F. Jing[3], M. John[54], D. Johnson[54], C.R. Jones[46], C. Joram[37], B. Jost[37], M. Kaballo[9], S. Kandybei[42], M. Karacson[37], T.M. Karbach[37], I.R. Kenyon[44], U. Kerzel[37], T. Ketel[41], A. Keune[38], B. Khanji[20], O. Kochebina[7], I. Komarov[38], R.F. Koopman[41], P. Koppenburg[40], M. Korolev[31], A. Kozlinskiy[40], L. Kravchuk[32], K. Kreplin[11], M. Kreps[47], G. Krocker[11], P. Krokovny[33], F. Kruse[9], M. Kucharczyk[20,25,j], V. Kudryavtsev[33], T. Kvaratskheliya[30,37], V.N. La Thi[38], D. Lacarrere[37], G. Lafferty[53], A. Lai[15], D. Lambert[49], R.W. Lambert[41], E. Lanciotti[37], G. Lanfranchi[18], C. Langenbruch[37], T. Latham[47], C. Lazzeroni[44], R. Le Gac[6], J. van Leerdam[40], J.-P. Lees[4], R. Lefèvre[5], A. Leflat[31], J. Lefrançois[7], S. Leo[22], O. Leroy[6], T. Lesiak[25], B. Leverington[11], Y. Li[3], L. Li Gioi[5], M. Liles[51], R. Lindner[37], C. Linn[11], B. Liu[3], G. Liu[37], S. Lohn[37], I. Longstaff[50], J.H. Lopes[2], E. Lopez Asamar[35], N. Lopez-March[38], H. Lu[3], D. Lucchesi[21,q], J. Luisier[38], H. Luo[49], F. Machefert[7], I.V. Machikhiliyan[4,30], F. Maciuc[28], O. Maev[29,37], S. Malde[54], G. Manca[15,d], G. Mancinelli[6], U. Marconi[14], R. Märki[38], J. Marks[11], G. Martellotti[24], A. Martens[8], L. Martin[54], A. Martín Sánchez[7], M. Martinelli[40], D. Martinez Santos[41], D. Martins Tostes[2], A. Massafferri[1], R. Matev[37], Z. Mathe[37], C. Matteuzzi[20], E. Maurice[6], A. Mazurov[16,32,37,e], J. McCarthy[44], A. McNab[53], R. McNulty[12], B. Meadows[56,54], F. Meier[9], M. Meissner[11], M. Merk[40], D.A. Milanes[8], M.-N. Minard[4], J. Molina Rodriguez[58], S. Monteil[5], D. Moran[53], P. Morawski[25], M.J. Morello[22,s], R. Mountain[57], I. Mous[40], F. Muheim[49], K. Müller[39], R. Muresan[28], B. Muryn[26], B. Muster[38], P. Naik[45], T. Nakada[38], R. Nandakumar[48], I. Nasteva[1], M. Needham[49], N. Neufeld[37], A.D. Nguyen[38], T.D. Nguyen[38], C. Nguyen-Mau[38,p], M. Nicol[7], V. Niess[5], R. Niet[9], N. Nikitin[31], T. Nikodem[11], A. Nomerotski[54], A. Novoselov[34], A. Oblakowska-Mucha[26], V. Obraztsov[34], S. Oggero[40], S. Ogilvy[50], O. Okhrimenko[43], R. Oldeman[15,d], M. Orlandea[28], J.M. Otalora Goicochea[2], P. Owen[52], A. Oyanguren [35,o], B.K. Pal[57], A. Palano[13,b], M. Palutan[18], J. Panman[37], A. Papanestis[48], M. Pappagallo[50], C. Parkes[53], C.J. Parkinson[52], G. Passaleva[17], G.D. Patel[51], M. Patel[52], G.N. Patrick[48], C. Patrignani[19,i], C. Pavel-Nicorescu[28], A. Pazos Alvarez[36], A. Pellegrino[40], G. Penso[24,l], M. Pepe Altarelli[37], S. Perazzini[14,c], D.L. Perego[20,j], E. Perez Trigo[36], A. Pérez-Calero Yzquierdo[35], P. Perret[5], M. Perrin-Terrin[6], G. Pessina[20], K. Petridis[52], A. Petrolini[19,i], A. Phan[57], E. Picatoste Olloqui[35], B. Pietrzyk[4], T. Pilař[47], D. Pinci[24], S. Playfer[49], M. Plo Casasus[36], F. Polci[8], G. Polok[25], A. Poluektov[47,33], E. Polycarpo[2], A. Popov[34], D. Popov[10], B. Popovici[28], C. Potterat[35], A. Powell[54], J. Prisciandaro[38], V. Pugatch[43], A. Puig Navarro[38], G. Punzi[22,r], W. Qian[4], J.H. Rademacker[45], B. Rakotomiaramanana[38], M.S. Rangel[2], I. Raniuk[42], N. Rauschmayr[37], G. Raven[41], S. Redford[54], M.M. Reid[47], A.C. dos Reis[1], S. Ricciardi[48], A. Richards[52], K. Rinnert[51], V. Rives Molina[35], D.A. Roa Romero[5], P. Robbe[7], E. Rodrigues[53], P. Rodriguez Perez[36], S. Roiser[37], V. Romanovsky[34], A. Romero Vidal[36], J. Rouvinet[38], T. Ruf[37], F. Ruffini[22], H. Ruiz[35], P. Ruiz Valls[35,o], G. Sabatino[24,k], J.J. Saborido Silva[36], N. Sagidova[29], P. Sail[50], B. Saitta[15,d], V. Salustino Guimaraes[2], C. Salzmann[39], B. Sanmartin Sedes[36], M. Sannino[19,i], R. Santacesaria[24], C. Santamarina Rios[36], E. Santovetti[23,k], M. Sapunov[6], A. Sarti[18,l], C. Satriano[24,m], A. Satta[23], M. Savrie[16,e], D. Savrina[30,31], P. Schaack[52], M. Schiller[41], H. Schindler[37], M. Schlupp[9], M. Schmelling[10], B. Schmidt[37], O. Schneider[38], A. Schopper[37], M.-H. Schune[7], R. Schwemmer[37], B. Sciascia[18], A. Sciubba[24], M. Seco[36], A. Semennikov[30], K. Senderowska[26], I. Sepp[52], N. Serra[39], J. Serrano[6], P. Seyfert[11], M. Shapkin[34], I. Shapoval[16,42], P. Shatalov[30], Y. Shcheglov[29], T. Shears[51,37], L. Shekhtman[33], O. Shevchenko[42], V. Shevchenko[30], A. Shires[52], R. Silva Coutinho[47], T. Skwarnicki[57], N.A. Smith[51], E. Smith[54,48], M. Smith[53], M.D. Sokoloff[56], F.J.P. Soler[50], F. Soomro[18], D. Souza[45], B. Souza De Paula[2], B. Spaan[9], A. Sparkes[49], P. Spradlin[50], F. Stagni[37], S. Stahl[11], O. Steinkamp[39], S. Stoica[28],

S. Stone[57], B. Storaci[39], M. Straticiuc[28], U. Straumann[39], V.K. Subbiah[37], L. Sun[56], S. Swientek[9], V. Syropoulos[41], M. Szczekowski[27], P. Szczypka[38,37], T. Szumlak[26], S. T'Jampens[4], M. Teklishyn[7], E. Teodorescu[28], F. Teubert[37], C. Thomas[54], E. Thomas[37], J. van Tilburg[11], V. Tisserand[4], M. Tobin[38], S. Tolk[41], D. Tonelli[37], S. Topp-Joergensen[54], N. Torr[54], E. Tournefier[4,52], S. Tourneur[38], M.T. Tran[38], M. Tresch[39], A. Tsaregorodtsev[6], P. Tsopelas[40], N. Tuning[40], M. Ubeda Garcia[37], A. Ukleja[27], D. Urner[53], U. Uwer[11], V. Vagnoni[14], G. Valenti[14], R. Vazquez Gomez[35], P. Vazquez Regueiro[36], S. Vecchi[16], J.J. Velthuis[45], M. Veltri[17,g], G. Veneziano[38], M. Vesterinen[37], B. Viaud[7], D. Vieira[2], X. Vilasis-Cardona[35,n], A. Vollhardt[39], D. Volyanskyy[10], D. Voong[45], A. Vorobyev[29], V. Vorobyev[33], C. Voß[59], H. Voss[10], R. Waldi[59], R. Wallace[12], S. Wandernoth[11], J. Wang[57], D.R. Ward[46], N.K. Watson[44], A.D. Webber[53], D. Websdale[52], M. Whitehead[47], J. Wicht[37], J. Wiechczynski[25], D. Wiedner[11], L. Wiggers[40], G. Wilkinson[54], M.P. Williams[47,48], M. Williams[55], F.F. Wilson[48], J. Wishahi[9], M. Witek[25], S.A. Wotton[46], S. Wright[46], S. Wu[3], K. Wyllie[37], Y. Xie[49,37], F. Xing[54], Z. Xing[57], Z. Yang[3], R. Young[49], X. Yuan[3], O. Yushchenko[34], M. Zangoli[14], M. Zavertyaev[10,a], F. Zhang[3], L. Zhang[57], W.C. Zhang[12], Y. Zhang[3], A. Zhelezov[11], A. Zhokhov[30], L. Zhong[3], A. Zvyagin[37].

[1] *Centro Brasileiro de Pesquisas Físicas (CBPF), Rio de Janeiro, Brazil*
[2] *Universidade Federal do Rio de Janeiro (UFRJ), Rio de Janeiro, Brazil*
[3] *Center for High Energy Physics, Tsinghua University, Beijing, China*
[4] *LAPP, Université de Savoie, CNRS/IN2P3, Annecy-Le-Vieux, France*
[5] *Clermont Université, Université Blaise Pascal, CNRS/IN2P3, LPC, Clermont-Ferrand, France*
[6] *CPPM, Aix-Marseille Université, CNRS/IN2P3, Marseille, France*
[7] *LAL, Université Paris-Sud, CNRS/IN2P3, Orsay, France*
[8] *LPNHE, Université Pierre et Marie Curie, Université Paris Diderot, CNRS/IN2P3, Paris, France*
[9] *Fakultät Physik, Technische Universität Dortmund, Dortmund, Germany*
[10] *Max-Planck-Institut für Kernphysik (MPIK), Heidelberg, Germany*
[11] *Physikalisches Institut, Ruprecht-Karls-Universität Heidelberg, Heidelberg, Germany*
[12] *School of Physics, University College Dublin, Dublin, Ireland*
[13] *Sezione INFN di Bari, Bari, Italy*
[14] *Sezione INFN di Bologna, Bologna, Italy*
[15] *Sezione INFN di Cagliari, Cagliari, Italy*
[16] *Sezione INFN di Ferrara, Ferrara, Italy*
[17] *Sezione INFN di Firenze, Firenze, Italy*
[18] *Laboratori Nazionali dell'INFN di Frascati, Frascati, Italy*
[19] *Sezione INFN di Genova, Genova, Italy*
[20] *Sezione INFN di Milano Bicocca, Milano, Italy*
[21] *Sezione INFN di Padova, Padova, Italy*
[22] *Sezione INFN di Pisa, Pisa, Italy*
[23] *Sezione INFN di Roma Tor Vergata, Roma, Italy*
[24] *Sezione INFN di Roma La Sapienza, Roma, Italy*
[25] *Henryk Niewodniczanski Institute of Nuclear Physics Polish Academy of Sciences, Kraków, Poland*
[26] *AGH - University of Science and Technology, Faculty of Physics and Applied Computer Science, Kraków, Poland*
[27] *National Center for Nuclear Research (NCBJ), Warsaw, Poland*
[28] *Horia Hulubei National Institute of Physics and Nuclear Engineering, Bucharest-Magurele, Romania*
[29] *Petersburg Nuclear Physics Institute (PNPI), Gatchina, Russia*
[30] *Institute of Theoretical and Experimental Physics (ITEP), Moscow, Russia*
[31] *Institute of Nuclear Physics, Moscow State University (SINP MSU), Moscow, Russia*
[32] *Institute for Nuclear Research of the Russian Academy of Sciences (INR RAN), Moscow, Russia*
[33] *Budker Institute of Nuclear Physics (SB RAS) and Novosibirsk State University, Novosibirsk, Russia*

[34] *Institute for High Energy Physics (IHEP), Protvino, Russia*
[35] *Universitat de Barcelona, Barcelona, Spain*
[36] *Universidad de Santiago de Compostela, Santiago de Compostela, Spain*
[37] *European Organization for Nuclear Research (CERN), Geneva, Switzerland*
[38] *Ecole Polytechnique Fédérale de Lausanne (EPFL), Lausanne, Switzerland*
[39] *Physik-Institut, Universität Zürich, Zürich, Switzerland*
[40] *Nikhef National Institute for Subatomic Physics, Amsterdam, The Netherlands*
[41] *Nikhef National Institute for Subatomic Physics and VU University Amsterdam, Amsterdam, The Netherlands*
[42] *NSC Kharkiv Institute of Physics and Technology (NSC KIPT), Kharkiv, Ukraine*
[43] *Institute for Nuclear Research of the National Academy of Sciences (KINR), Kyiv, Ukraine*
[44] *University of Birmingham, Birmingham, United Kingdom*
[45] *H.H. Wills Physics Laboratory, University of Bristol, Bristol, United Kingdom*
[46] *Cavendish Laboratory, University of Cambridge, Cambridge, United Kingdom*
[47] *Department of Physics, University of Warwick, Coventry, United Kingdom*
[48] *STFC Rutherford Appleton Laboratory, Didcot, United Kingdom*
[49] *School of Physics and Astronomy, University of Edinburgh, Edinburgh, United Kingdom*
[50] *School of Physics and Astronomy, University of Glasgow, Glasgow, United Kingdom*
[51] *Oliver Lodge Laboratory, University of Liverpool, Liverpool, United Kingdom*
[52] *Imperial College London, London, United Kingdom*
[53] *School of Physics and Astronomy, University of Manchester, Manchester, United Kingdom*
[54] *Department of Physics, University of Oxford, Oxford, United Kingdom*
[55] *Massachusetts Institute of Technology, Cambridge, MA, United States*
[56] *University of Cincinnati, Cincinnati, OH, United States*
[57] *Syracuse University, Syracuse, NY, United States*
[58] *Pontifícia Universidade Católica do Rio de Janeiro (PUC-Rio), Rio de Janeiro, Brazil, associated to* [2]
[59] *Institut für Physik, Universität Rostock, Rostock, Germany, associated to* [11]

[a] *P.N. Lebedev Physical Institute, Russian Academy of Science (LPI RAS), Moscow, Russia*
[b] *Università di Bari, Bari, Italy*
[c] *Università di Bologna, Bologna, Italy*
[d] *Università di Cagliari, Cagliari, Italy*
[e] *Università di Ferrara, Ferrara, Italy*
[f] *Università di Firenze, Firenze, Italy*
[g] *Università di Urbino, Urbino, Italy*
[h] *Università di Modena e Reggio Emilia, Modena, Italy*
[i] *Università di Genova, Genova, Italy*
[j] *Università di Milano Bicocca, Milano, Italy*
[k] *Università di Roma Tor Vergata, Roma, Italy*
[l] *Università di Roma La Sapienza, Roma, Italy*
[m] *Università della Basilicata, Potenza, Italy*
[n] *LIFAELS, La Salle, Universitat Ramon Llull, Barcelona, Spain*
[o] *IFIC, Universitat de Valencia-CSIC, Valencia, Spain*
[p] *Hanoi University of Science, Hanoi, Viet Nam*
[q] *Università di Padova, Padova, Italy*
[r] *Università di Pisa, Pisa, Italy*
[s] *Scuola Normale Superiore, Pisa, Italy*

1 Introduction

The observation of neutrino oscillations was the first evidence for lepton flavour violation (LFV). As a consequence, the introduction of mass terms for neutrinos in the Standard Model (SM) implies that LFV exists also in the charged sector, but with branching fractions smaller than $\sim 10^{-40}$ [1,2]. Physics beyond the Standard Model (BSM) could significantly enhance these branching fractions. Many BSM theories predict enhanced LFV in τ^- decays with respect to μ^- decays[1], with branching fractions within experimental reach [3]. To date, no charged LFV decays such as $\mu^- \to e^-\gamma$, $\mu^- \to e^-e^+e^-$, $\tau^- \to \ell^-\gamma$ and $\tau^- \to \ell^-\ell^+\ell^-$ (with $\ell^- = e^-, \mu^-$) have been observed [4]. Baryon number violation (BNV) is believed to have occurred in the early universe, although the mechanism is unknown. BNV in charged lepton decays automatically implies lepton number and lepton flavour violation, with angular momentum conservation requiring the change $|\Delta(B-L)| = 0$ or 2, where B and L are the net baryon and lepton numbers. The SM and most of its extensions [1] require $|\Delta(B-L)| = 0$. Any observation of BNV or charged LFV would be a clear sign for BSM physics, while a lowering of the experimental upper limits on branching fractions would further constrain the parameter spaces of BSM models.

In this Letter we report on searches for the LFV decay $\tau^- \to \mu^-\mu^+\mu^-$ and the LFV and BNV decay modes $\tau^- \to \bar{p}\mu^+\mu^-$ and $\tau^- \to p\mu^-\mu^-$ at LHCb [5]. The inclusive τ^- production cross-section at the LHC is relatively large, at about 80 μb (approximately 80% of which comes from $D_s^- \to \tau^-\bar{\nu}_\tau$), estimated using the $b\bar{b}$ and $c\bar{c}$ cross-sections measured by LHCb [6,7] and the inclusive $b \to \tau$ and $c \to \tau$ branching fractions [8]. The $\tau^- \to \mu^-\mu^+\mu^-$ and $\tau \to p\mu\mu$ decay modes[2] are of particular interest at LHCb, since muons provide clean signatures in the detector and the ring-imaging Cherenkov (RICH) detectors give excellent identification of protons.

This Letter presents the first results on the $\tau^- \to \mu^-\mu^+\mu^-$ decay mode from a hadron collider and demonstrates an experimental sensitivity at LHCb, with data corresponding to an integrated luminosity of $1.0\,\text{fb}^{-1}$, that approaches the current best experimental upper limit, from Belle, $\mathcal{B}(\tau^- \to \mu^-\mu^+\mu^-) < 2.1 \times 10^{-8}$ at 90% confidence level (CL) [9]. BaBar and Belle have searched for BNV τ decays with $|\Delta(B-L)| = 0$ and $|\Delta(B-L)| = 2$ using the modes $\tau^- \to \Lambda h^-$ and $\bar{\Lambda} h^-$ (with $h^- = \pi^-, K^-$), and upper limits on branching fractions of order 10^{-7} were obtained [4]. BaBar has also searched for the B meson decays $B^0 \to \Lambda_c^+ l^-$, $B^- \to \Lambda l^-$ (both having $|\Delta(B-L)| = 0$) and $B^- \to \bar{\Lambda} l^-$ ($|\Delta(B-L)| = 2$), obtaining upper limits at 90% CL on branching fractions in the range $(3.2 - 520) \times 10^{-8}$ [10]. The two BNV τ decays presented here, $\tau^- \to \bar{p}\mu^+\mu^-$ and $\tau^- \to p\mu^-\mu^-$, have $|\Delta(B-L)| = 0$ but they could have rather different BSM interpretations; they have not been studied by any previous experiment.

In this analysis the LHCb data sample from 2011, corresponding to an integrated luminosity of $1.0\,\text{fb}^{-1}$ collected at $\sqrt{s} = 7\,\text{TeV}$, is used. Selection criteria are implemented for the three signal modes, $\tau^- \to \mu^-\mu^+\mu^-$, $\tau^- \to \bar{p}\mu^+\mu^-$ and $\tau^- \to p\mu^-\mu^-$, and for the calibration and normalisation channel, which is $D_s^- \to \phi\pi^-$ followed by $\phi \to \mu^+\mu^-$, referred

[1]The inclusion of charge conjugate processes is implied throughout this Letter.

[2]In the following $\tau \to p\mu\mu$ refers to both the $\tau^- \to \bar{p}\mu^+\mu^-$ and $\tau^- \to p\mu^-\mu^-$ channels.

to in the following as $D_s^- \to \phi(\mu^+\mu^-)\pi^-$. These initial, cut-based selections are designed to keep good efficiency for signal whilst reducing the dataset to a manageable level. To avoid potential bias, $\mu^-\mu^+\mu^-$ and $p\mu\mu$ candidates with mass within $\pm 30\,\text{MeV}/c^2$ ($\approx 3\sigma_m$) of the τ mass are initially blinded from the analysis, where σ_m denotes the expected mass resolution. For the 3μ channel, discrimination between potential signal and background is performed using a three-dimensional binned distribution in two likelihood variables and the mass of the τ candidate. One likelihood variable is based on the three-body decay topology and the other on muon identification. For the $\tau \to p\mu\mu$ channels, the use of the second likelihood function is replaced by cuts on the proton and muon particle identification (PID) variables. The analysis strategy and limit-setting procedure are similar to those used for the LHCb analyses of the $B_s^0 \to \mu^+\mu^-$ and $B^0 \to \mu^+\mu^-$ channels [11, 12].

2 Detector and triggers

The LHCb detector [5] is a single-arm forward spectrometer covering the pseudorapidity range $2 < \eta < 5$, designed for the study of particles containing b or c quarks. The detector includes a high precision tracking system consisting of a silicon-strip vertex detector surrounding the pp interaction region, a large-area silicon-strip detector located upstream of a dipole magnet with a bending power of about 4 Tm, and three stations of silicon-strip detectors and straw drift tubes placed downstream. The combined tracking system has momentum resolution $\Delta p/p$ that varies from 0.4% at $5\,\text{GeV}/c$ to 0.6% at $100\,\text{GeV}/c$, and impact parameter resolution of 20 µm for tracks with high transverse momentum (p_T). Charged hadrons are identified using two RICH detectors. Photon, electron and hadron candidates are identified by a calorimeter system consisting of scintillating-pad and preshower detectors, an electromagnetic calorimeter and a hadronic calorimeter. Muons are identified by a system composed of alternating layers of iron and multiwire proportional chambers.

The trigger [13] consists of a hardware stage, based on information from the calorimeter and muon systems, followed by a software stage that applies a full event reconstruction. The hardware trigger selects muons with $p_\text{T} > 1.48\,\text{GeV}/c$. The software trigger requires a two-, three- or four-track secondary vertex with a high sum of the p_T of the tracks and a significant displacement from the primary pp interaction vertices (PVs). At least one track should have $p_\text{T} > 1.7\,\text{GeV}/c$ and impact parameter chi-squared (IP χ^2), with respect to the pp collision vertex, greater than 16. The IP χ^2 is defined as the difference between the χ^2 of the PV reconstructed with and without the track under consideration. A multivariate algorithm is used for the identification of secondary vertices.

For the simulation, pp collisions are generated using Pythia 6.4 [14] with a specific LHCb configuration [15]. Particle decays are described by EvtGen [16] in which final-state radiation is generated using Photos [17]. For the three signal τ decay channels, the final-state particles are distributed according to three-body phase space. The interaction of the generated particles with the detector, and its response, are implemented using the Geant4 toolkit [18] as described in Ref. [19].

3 Signal candidate selection

The signal and normalisation channels have the same topology, the signature of which is a vertex displaced from the PV, having three tracks that are reconstructed to give a mass close to that of the τ lepton (or D_s meson for the normalisation channel). In order to discriminate against background, well-reconstructed and well-identified muon, pion and proton tracks are required, with selections on track quality criteria and a requirement of $p_{\mathrm{T}} > 300$ MeV/c. Furthermore, for the $\tau \to p\mu\mu$ signal and normalisation channels the muon and proton candidates must pass loose PID requirements and the combined p_{T} of the three-track system is required to be greater than $4\,\mathrm{GeV}/c$. All selected tracks are required to have IP $\chi^2 > 9$. The fitted three-track vertex has to be of good quality, with a fit $\chi^2 < 15$, and the measured decay time, t, of the candidate forming the vertex has to be compatible with that of a heavy meson or tau lepton ($ct > 100\,\mu\mathrm{m}$). Since the Q-values in decays of charm mesons to τ are relatively small, poorly reconstructed candidates are removed by a cut on the pointing angle between the momentum vector of the three-track system and the line joining the primary and secondary vertices. In the $\tau^- \to \mu^-\mu^+\mu^-$ channel, signal candidates with a $\mu^+\mu^-$ mass within $\pm 20\,\mathrm{MeV}/c^2$ of the ϕ meson mass are removed, and to eliminate irreducible background near the signal region arising from the decay $D_s^- \to \eta(\mu^+\mu^-\gamma)\mu^-\bar{\nu}_\mu$, candidates with a $\mu^+\mu^-$ mass combination below $450\,\mathrm{MeV}/c^2$ are also rejected (see Section 6). Finally, to remove potential contamination from pairs of reconstructed tracks that arise from the same particle, same-sign muon pairs with mass lower than $250\,\mathrm{MeV}/c^2$ are removed in both the $\tau^- \to \mu^-\mu^+\mu^-$ and $\tau^- \to p\mu^-\mu^-$ channels. The signal regions are defined by $\pm 20\,\mathrm{MeV}/c^2$ ($\approx 2\sigma_m$) windows around the nominal τ mass, but candidates within wide mass windows, of $\pm 400\,\mathrm{MeV}/c^2$ for $\tau^- \to \mu^-\mu^+\mu^-$ decays and $\pm 250\,\mathrm{MeV}/c^2$ for $\tau \to p\mu\mu$ decays, are kept to allow evaluation of the background contributions in the signal regions. A mass window of $\pm 20\,\mathrm{MeV}/c^2$ is also used to define the signal region for the $D_s^- \to \phi(\mu^+\mu^-)\pi^-$ channel, with the $\mu^+\mu^-$ mass required to be within $\pm 20\,\mathrm{MeV}/c^2$ of the ϕ meson mass.

4 Signal and background discrimination

After the selection each τ candidate is given a probability to be signal or background according to the values of several likelihoods. For $\tau^- \to \mu^-\mu^+\mu^-$ three likelihoods are used: a three-body likelihood, $\mathcal{M}_{\mathrm{3body}}$, a PID likelihood, $\mathcal{M}_{\mathrm{PID}}$, and an invariant mass likelihood. The likelihood $\mathcal{M}_{\mathrm{3body}}$ uses the properties of the reconstructed τ decay to distinguish displaced three-body decays from N-body decays (with $N > 3$) and combinations of tracks from different vertices. Variables used include the vertex quality and its displacement from the PV, and the IP and fit χ^2 values of the tracks. The likelihood $\mathcal{M}_{\mathrm{PID}}$ quantifies the compatibility of each of the three particles with the muon hypothesis using information from the RICH detectors, the calorimeters and the muon stations; the value of $\mathcal{M}_{\mathrm{PID}}$ is taken as the smallest one of the three muon candidates. For $\tau \to p\mu\mu$, the use of $\mathcal{M}_{\mathrm{PID}}$ is replaced by cuts on PID quantities. The invariant mass likelihood uses the reconstructed mass of the τ candidate to help discriminate between signal and background.

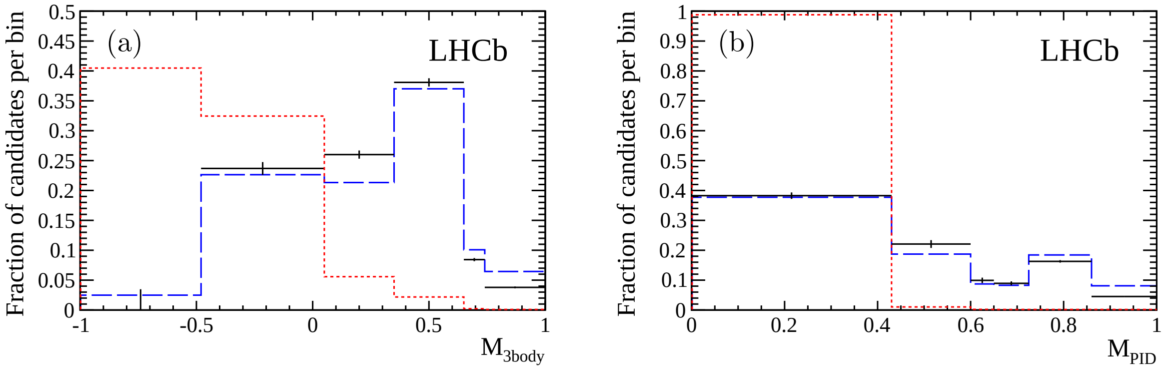

Figure 1: Distribution of (a) $\mathcal{M}_{\rm 3body}$ and (b) $\mathcal{M}_{\rm PID}$ for $\tau^- \to \mu^-\mu^+\mu^-$ where the binning corresponds to that used in the limit calculation. The short dashed (red) lines show the response of the data sidebands, whilst the long dashed (blue) and solid (black) lines show the response of simulated signal events before and after calibration. Note that in both cases the lowest likelihood bin is later excluded from the analysis.

For the $\mathcal{M}_{\rm 3body}$ likelihood a boosted decision tree [20] is used, with the AdaBoost algorithm [21], and is implemented via the TMVA [22] toolkit. It is trained using signal and background samples, both from simulation, where the composition of the background is a mixture of $b\bar{b} \to \mu\mu X$ and $c\bar{c} \to \mu\mu X$ according to their relative abundance as measured in data. The $\mathcal{M}_{\rm PID}$ likelihood uses a neural network, which is also trained on simulated events. The probability density function shapes are calibrated using the $D_s^- \to \phi(\mu^+\mu^-)\pi^-$ control channel and $J/\psi \to \mu^+\mu^-$ data for the $\mathcal{M}_{\rm 3body}$ and $\mathcal{M}_{\rm PID}$ likelihoods, respectively. The shape of the signal mass spectrum is modelled using $D_s^- \to \phi(\mu^+\mu^-)\pi^-$ data. The $\mathcal{M}_{\rm 3body}$ response as determined using the training from the $\tau^- \to \mu^-\mu^+\mu^-$ samples is used also for the $\tau \to p\mu\mu$ analyses.

For the $\mathcal{M}_{\rm 3body}$ and $\mathcal{M}_{\rm PID}$ likelihoods the binning is chosen such that the separation power between the background-only and signal-plus-background hypotheses is maximised, whilst minimising the number of bins. For the $\mathcal{M}_{\rm 3body}$ likelihood the optimum number of bins is found to be six for the $\tau^- \to \mu^-\mu^+\mu^-$ analysis and five for $\tau \to p\mu\mu$, while for the $\mathcal{M}_{\rm PID}$ likelihood the optimum number of bins is found to be five. The lowest bins in $\mathcal{M}_{\rm 3body}$ and $\mathcal{M}_{\rm PID}$ do not contribute to the sensitivity and are later excluded from the analyses. The distributions of the two likelihoods, along with their binning schemes, are shown in Fig. 1 for the $\tau^- \to \mu^-\mu^+\mu^-$ analysis.

For the $\tau \to p\mu\mu$ analysis, further cuts on the muon and proton PID hypotheses are used instead of $\mathcal{M}_{\rm PID}$ and are optimised, for a 2σ significance, on simulated signal events and data sidebands using the figure of merit from Ref. [23], with the distributions of the PID variables corrected according to those observed in data. The expected shapes of the invariant mass spectra for the $\tau^- \to \mu^-\mu^+\mu^-$ and $\tau \to p\mu\mu$ signals, with the appropriate selections applied, are taken from fits to the $D_s^- \to \phi(\mu^+\mu^-)\pi^-$ control channel in data as shown in Fig. 2. The signal distributions are modelled with the sum of two Gaussian functions with a common mean, where the narrower Gaussian contributes 70% of the total

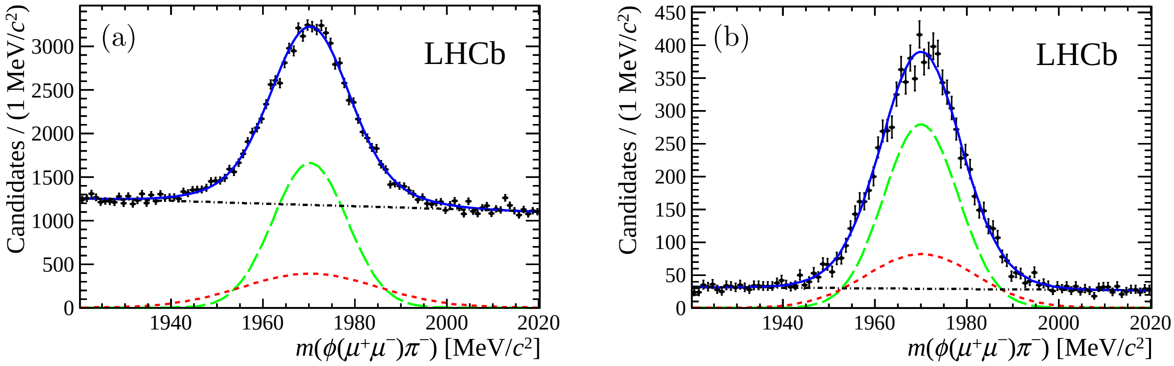

Figure 2: Invariant mass distribution of $\phi(\mu^+\mu^-)\pi^-$ after (a) the $\tau^- \to \mu^-\mu^+\mu^-$ selection and (b) the $\tau \to p\mu\mu$ selection and PID cuts. The solid (blue) lines show the overall fits, the long dashed (green) and short dashed (red) lines show the two Gaussian components of the signal and the dot dashed (black) lines show the backgrounds.

signal yield, while the combinatorial backgrounds are modelled with linear functions. The expected widths of the τ signals in data are taken from simulation, scaled by the ratio of the widths of the D_s^- peaks in data and simulation. The data are divided into eight equally spaced bins in the $\pm 20\,\text{MeV}/c^2$ mass window around the nominal τ mass.

5 Normalisation

To measure the signal branching fraction for the decay $\tau^- \to \mu^-\mu^+\mu^-$ (and similarly for $\tau \to p\mu\mu$) we normalise to the $D_s^- \to \phi(\mu^+\mu^-)\pi^-$ calibration channel using

$$\begin{aligned}
&\mathcal{B}(\tau^- \to \mu^-\mu^+\mu^-) \\
&\quad = \mathcal{B}(D_s^- \to \phi(\mu^+\mu^-)\pi^-) \times \frac{f_\tau^{D_s}}{\mathcal{B}(D_s^- \to \tau^-\bar{\nu}_\tau)} \times \frac{\epsilon_{\text{cal}}^{\text{REC\&SEL}}}{\epsilon_{\text{sig}}^{\text{REC\&SEL}}} \times \frac{\epsilon_{\text{cal}}^{\text{TRIG}}}{\epsilon_{\text{sig}}^{\text{TRIG}}} \times \frac{N_{\text{sig}}}{N_{\text{cal}}} \\
&\quad = \alpha \times N_{\text{sig}}\,,
\end{aligned} \tag{1}$$

where α is the overall normalisation factor and N_{sig} is the number of observed signal events. The branching fraction $\mathcal{B}(D_s^- \to \tau^-\bar{\nu}_\tau)$ is taken from Ref. [24]. The quantity $f_\tau^{D_s}$ is the fraction of τ leptons that originate from D_s^- decays, calculated using the $b\bar{b}$ and $c\bar{c}$ cross-sections as measured by LHCb [6, 7] and the inclusive $b \to \tau$, $c \to \tau$, $b \to D_s$ and $c \to D_s$ branching fractions [8]. The corresponding expression for the $\tau \to p\mu\mu$ decay is identical except for the inclusion of a further term, $\epsilon_{\text{cal}}^{\text{PID}}/\epsilon_{\text{sig}}^{\text{PID}}$, to account for the effect of the PID cuts.

The reconstruction and selection efficiencies, $\epsilon^{\text{REC\&SEL}}$, are products of the detector acceptances for the particular decays, the muon identification efficiencies and the selection efficiencies. The combined muon identification and selection efficiency is determined from the yield of simulated events after the full selections have been applied. In the sample of simulated events, the track IPs are smeared to describe the secondary-vertex resolution of the data. Furthermore, the events are given weights to adjust the prompt and non-prompt b and c particle production fractions to the latest measurements [8]. The difference in the result if the weights are varied within their uncertainties is assigned as a systematic uncertainty. The ratio of efficiencies is corrected to account for the differences between data and simulation in efficiencies of track reconstruction, muon identification, the $\phi(1020)$ mass window cut in the normalisation channel and the τ mass window cut, with all associated systematic uncertainties included. The removal of candidates in the least sensitive bins in the $\mathcal{M}_{\rm 3body}$ and $\mathcal{M}_{\rm PID}$ classifiers is also taken into account.

The trigger efficiency for selected candidates, $\epsilon^{\rm TRIG}$, is evaluated from simulation while its systematic uncertainty is determined from the difference between trigger efficiencies of $B^- \to J/\psi K^-$ decays measured in data and in simulation.

For the $\tau \to p\mu\mu$ channels the PID efficiency for selected and triggered candidates, $\epsilon^{\rm PID}$, is calculated using data calibration samples of $J/\psi \to \mu^+\mu^-$ and $\Lambda \to p\pi^-$ decays, with the tracks weighted to match the kinematics of the signal and calibration channels. A systematic uncertainty of 1% per corrected final-state track is assigned [7], as well as a further 1% uncertainty to account for differences in the kinematic binning of the calibration samples between the analyses.

The branching fraction of the calibration channel is determined from a combination of known branching fractions using

$$\mathcal{B}(D_s^- \to \phi(\mu^+\mu^-)\pi^-) = \frac{\mathcal{B}(D_s^- \to \phi(K^+K^-)\pi^-)}{\mathcal{B}(\phi \to K^+K^-)}\mathcal{B}(\phi \to \mu^+\mu^-) = (1.33 \pm 0.12) \times 10^{-5}\,, \tag{2}$$

where $\mathcal{B}(\phi \to K^+K^-)$ and $\mathcal{B}(\phi \to \mu^+\mu^-)$ are taken from [8] and $\mathcal{B}(D_s^- \to \phi(K^+K^-)\pi^-)$ is taken from the BaBar amplitude analysis [25], which considers only the $\phi \to K^+K^-$ resonant part of the D_s^- decay. This is motivated by the negligible contribution of non-resonant $D_s^- \to \mu^+\mu^-\pi^-$ events seen in our data. The yields of $D_s^- \to \phi(\mu^+\mu^-)\pi^-$ candidates in data, $N_{\rm cal}$, are determined from the fits to reconstructed $\phi(\mu^+\mu^-)\pi^-$ mass distributions, shown in Fig. 2. The variations in the yields if the relative contributions of the two Gaussian components are varied in the fits are considered as systematic uncertainties. Table 1 gives a summary of all contributions to α; the uncertainties are taken to be uncorrelated.

Table 1: Terms entering in the normalisation factor α for $\tau^- \to \mu^-\mu^+\mu^-$, $\tau^- \to \bar{p}\mu^+\mu^-$ and $\tau^- \to p\mu^-\mu^-$, and their combined statistical and systematic uncertainties.

	$\tau^- \to \mu^-\mu^+\mu^-$	$\tau^- \to \bar{p}\mu^+\mu^-$	$\tau^- \to p\mu^-\mu^-$
$\mathcal{B}(D_s^- \to \phi(\mu^+\mu^-)\pi^-)$	$(1.33 \pm 0.12) \times 10^{-5}$		
$f_\tau^{D_s}$	0.78 ± 0.05		
$\mathcal{B}(D_s^- \to \tau^-\bar{\nu}_\tau)$	0.0561 ± 0.0024		
${\epsilon_{\rm cal}}^{\rm REC\&SEL}/{\epsilon_{\rm sig}}^{\rm REC\&SEL}$	1.49 ± 0.12	1.35 ± 0.12	1.36 ± 0.12
${\epsilon_{\rm cal}}^{\rm TRIG}/{\epsilon_{\rm sig}}^{\rm TRIG}$	0.753 ± 0.037	1.68 ± 0.10	2.03 ± 0.13
${\epsilon_{\rm cal}}^{\rm PID}/{\epsilon_{\rm sig}}^{\rm PID}$	n/a	1.43 ± 0.07	1.42 ± 0.08
$N_{\rm cal}$	$48\,076 \pm 840$	$8\,145 \pm 180$	
α	$(4.34 \pm 0.65) \times 10^{-9}$	$(7.4 \pm 1.2) \times 10^{-8}$	$(9.0 \pm 1.5) \times 10^{-8}$

6 Background studies

The background processes for the decay $\tau^- \to \mu^-\mu^+\mu^-$ consist mainly of decay chains of heavy mesons with three real muons in the final state or with one or two real muons in combination with two or one misidentified particles. These backgrounds vary smoothly in the mass spectra in the region of the signal channel. The most important peaking background channel is found to be $D_s^- \to \eta(\mu^+\mu^-\gamma)\mu^-\bar{\nu}_\mu$, about 80% of which is removed (see Section 3) by a cut on the dimuon mass. The small remaining background from this process is consistent with the smooth variation in the mass spectra of the other backgrounds in the mass range considered in the fit. Based on simulations, no peaking backgrounds are expected in the $\tau \to p\mu\mu$ analyses.

The expected numbers of background events within the signal region, for each bin in $\mathcal{M}_{\rm 3body}$, $\mathcal{M}_{\rm PID}$ (for $\tau^- \to \mu^-\mu^+\mu^-$) and mass, are evaluated by fitting the candidate mass spectra outside of the signal windows to an exponential function using an extended, unbinned maximum likelihood fit. The small differences obtained if the exponential curves are replaced by straight lines are included as systematic uncertainties. For $\tau^- \to \mu^-\mu^+\mu^-$ the data are fitted over the mass range $1600 - 1950\,{\rm MeV}/c^2$, while for $\tau \to p\mu\mu$ the fitted mass range is $1650 - 1900\,{\rm MeV}/c^2$, excluding windows around the expected signal mass of $\pm 30\,{\rm MeV}/c^2$ for $\mu^-\mu^+\mu^-$ and $\pm 20\,{\rm MeV}/c^2$ for $p\mu\mu$. The resulting fits to the data sidebands for a selection of bins for the three channels are shown in Fig. 3.

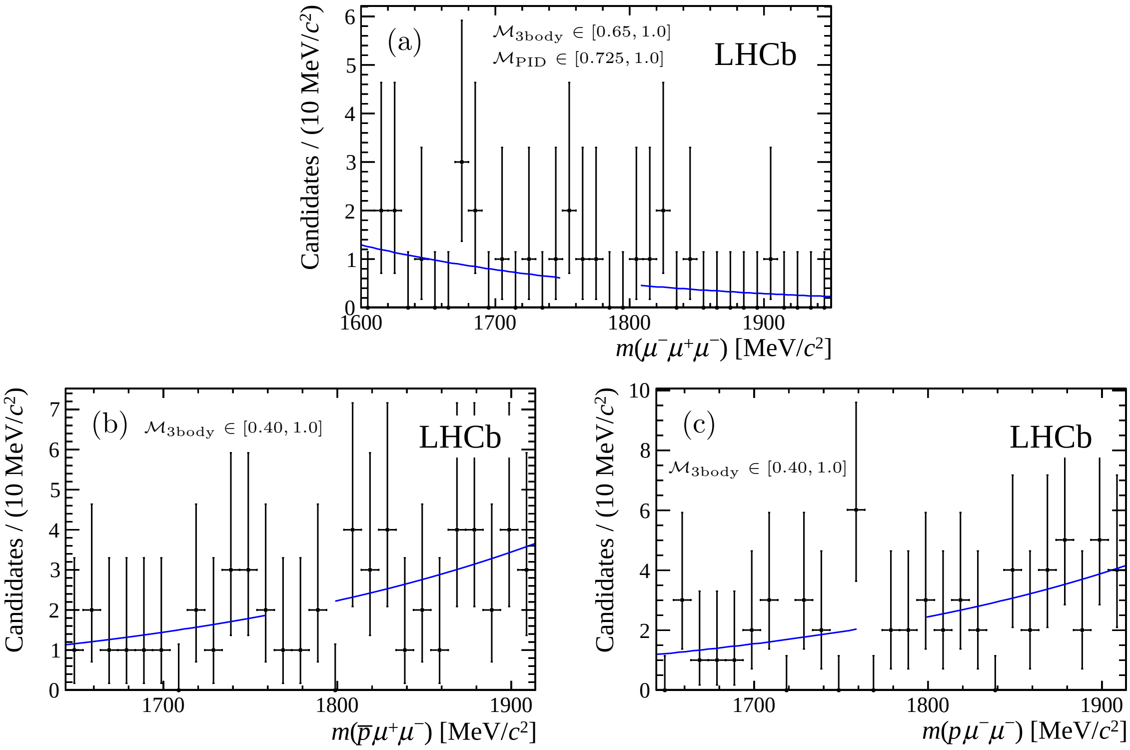

Figure 3: Invariant mass distributions and fits to the mass sidebands in data for (a) $\mu^+\mu^-\mu^-$ candidates in the four merged bins that contain the highest signal probabilities, (b) $\bar{p}\mu^+\mu^-$ candidates in the two merged bins with the highest signal probabilities, and (c) $p\mu^-\mu^-$ candidates in the two merged bins with the highest signal probabilities.

7 Results

Tables 2 and 3 give the expected and observed numbers of candidates for all three channels investigated, in each bin of the likelihood variables, where the uncertainties on the background likelihoods are used to compute the uncertainties on the expected numbers of events. No significant evidence for an excess of events is observed. Using the $\mathrm{CL_s}$ method as a statistical framework, the distributions of observed and expected $\mathrm{CL_s}$ values are calculated as functions of the assumed branching fractions. The aforementioned uncertainties and the uncertainties on the signal likelihoods and normalisation factors are included using the techniques described in Ref. [12]. The resulting distributions of $\mathrm{CL_s}$ values are shown in Fig. 4.

The expected limits at 90% (95%) CL for the branching fractions are

$$\begin{aligned}
\mathcal{B}(\tau^- \to \mu^-\mu^+\mu^-) &< 8.3\ (10.2) \times 10^{-8}, \\
\mathcal{B}(\tau^- \to \bar{p}\mu^+\mu^-) &< 4.6\ (5.9) \times 10^{-7}, \\
\mathcal{B}(\tau^- \to p\mu^-\mu^-) &< 5.4\ (6.9) \times 10^{-7},
\end{aligned}$$

while the observed limits at 90% (95%) CL are

$$\begin{aligned}
\mathcal{B}(\tau^- \to \mu^-\mu^+\mu^-) &< 8.0\ (9.8) \times 10^{-8}, \\
\mathcal{B}(\tau^- \to \bar{p}\mu^+\mu^-) &< 3.3\ (4.3) \times 10^{-7}, \\
\mathcal{B}(\tau^- \to p\mu^-\mu^-) &< 4.4\ (5.7) \times 10^{-7}.
\end{aligned}$$

All limits are given for the phase-space model of τ decays. For $\tau^- \to \mu^-\mu^+\mu^-$, the efficiency is found to vary by no more than 20% over the $\mu^-\mu^-$ mass range and by 10% over the $\mu^+\mu^-$ mass range. For $\tau \to p\mu\mu$, the efficiency varies by less than 20% over the dimuon mass range and less than 10% with $p\mu$ mass.

In summary, a first limit on the lepton flavour violating decay mode $\tau^- \to \mu^-\mu^+\mu^-$ has been obtained at a hadron collider. The result is compatible with previous limits and indicates that with the additional luminosity expected from the LHC over the coming years, the sensitivity of LHCb will become comparable with, or exceed, those of BaBar and Belle. First direct upper limits have been placed on the branching fractions for two τ decay modes that violate both baryon number and lepton flavour, $\tau^- \to \bar{p}\mu^+\mu^-$ and $\tau^- \to p\mu^-\mu^-$.

Table 2: Expected background candidate yields, with their systematic uncertainties, and observed candidate yields within the τ signal window in the different likelihood bins for the $\tau^- \to \mu^-\mu^+\mu^-$ analysis. The likelihood values for $\mathcal{M}_{\rm PID}$ range from 0 (most background-like) to +1 (most signal-like), while those for $\mathcal{M}_{\rm 3body}$ range from −1 (most background-like) to +1 (most signal-like). The lowest likelihood bins have been excluded from the analysis.

$\mathcal{M}_{\rm PID}$	$\mathcal{M}_{\rm 3body}$	Expected	Observed
0.43 − 0.6	$-0.48 - 0.05$	345.0 ± 6.7	409
	$0.05 - 0.35$	83.8 ± 3.3	68
	$0.35 - 0.65$	30.2 ± 2.0	35
	$0.65 - 0.74$	4.3 ± 0.8	2
	$0.74 - 1.0$	1.4 ± 0.4	1
0.6 − 0.65	$-0.48 - 0.05$	73.1 ± 3.1	64
	$0.05 - 0.35$	18.3 ± 1.5	15
	$0.35 - 0.65$	8.6 ± 1.1	7
	$0.65 - 0.74$	0.4 ± 0.1	0
	$0.74 - 1.0$	0.6 ± 0.2	2
0.65 − 0.725	$-0.48 - 0.05$	45.4 ± 2.4	51
	$0.05 - 0.35$	11.7 ± 1.2	6
	$0.35 - 0.65$	5.3 ± 0.8	3
	$0.65 - 0.74$	0.8 ± 0.2	1
	$0.74 - 1.0$	0.4 ± 0.1	0
0.725 − 0.86	$-0.48 - 0.05$	44.5 ± 2.4	62
	$0.05 - 0.35$	10.6 ± 1.2	13
	$0.35 - 0.65$	7.3 ± 1.0	7
	$0.65 - 0.74$	1.0 ± 0.2	2
	$0.74 - 1.0$	0.4 ± 0.1	0
0.86 − 1.0	$-0.48 - 0.05$	5.9 ± 0.9	7
	$0.05 - 0.35$	0.7 ± 0.2	1
	$0.35 - 0.65$	1.0 ± 0.2	1
	$0.65 - 0.74$	0.5 ± 0.0	0
	$0.74 - 1.0$	0.4 ± 0.1	0

Table 3: Expected background candidate yields, with their systematic uncertainties, and observed candidate yields within the τ mass window in the different likelihood bins for the $\tau \to p\mu\mu$ analysis. The likelihood values for $\mathcal{M}_{\rm 3body}$ range from -1 (most background-like) to $+1$ (most signal-like). The lowest likelihood bin has been excluded from the analysis.

	$\tau^- \to \bar{p}\mu^+\mu^-$		$\tau^- \to p\mu^-\mu^-$	
$\mathcal{M}_{\rm 3body}$	Expected	Observed	Expected	Observed
$-0.05 - 0.20$	37.9 ± 0.8	43	41.0 ± 0.9	41
$0.20 - 0.40$	12.6 ± 0.5	8	11.0 ± 0.5	13
$0.40 - 0.70$	6.76 ± 0.37	6	7.64 ± 0.39	10
$0.70 - 1.00$	0.96 ± 0.14	0	0.49 ± 0.12	0

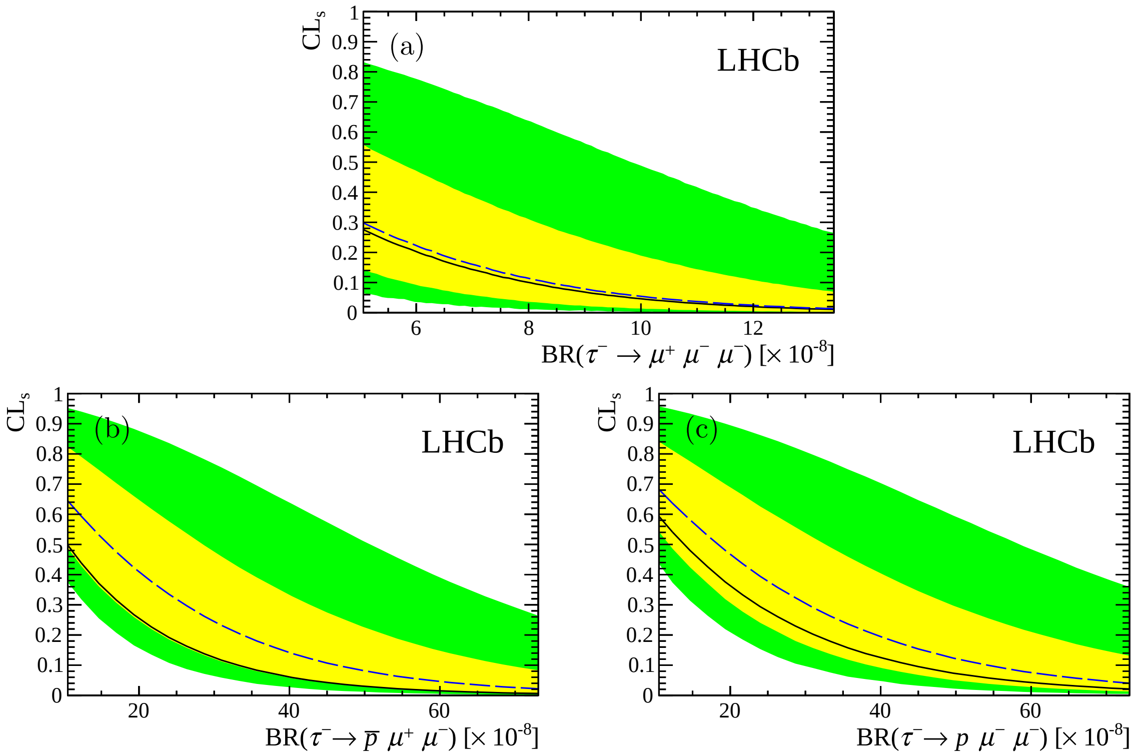

Figure 4: Distribution of $\mathrm{CL_s}$ values as functions of the assumed branching fractions, under the hypothesis to observe background events only, for (a) $\tau^- \to \mu^-\mu^+\mu^-$, (b) $\tau^- \to \bar{p}\mu^+\mu^-$ and (c) $\tau^- \to p\mu^-\mu^-$. The dashed lines indicate the expected curves and the solid lines the observed ones. The light (yellow) and dark (green) bands cover the regions of 68% and 95% confidence for the expected limits.

Acknowledgements

We express our gratitude to our colleagues in the CERN accelerator departments for the excellent performance of the LHC. We thank the technical and administrative staff at the LHCb institutes. We acknowledge support from CERN and from the national agencies: CAPES, CNPq, FAPERJ and FINEP (Brazil); NSFC (China); CNRS/IN2P3 and Region Auvergne (France); BMBF, DFG, HGF and MPG (Germany); SFI (Ireland); INFN (Italy); FOM and NWO (The Netherlands); SCSR (Poland); ANCS/IFA (Romania); MinES, Rosatom, RFBR and NRC "Kurchatov Institute" (Russia); MinECo, XuntaGal and GENCAT (Spain); SNSF and SER (Switzerland); NAS Ukraine (Ukraine); STFC (United Kingdom); NSF (USA). We also acknowledge the support received from the ERC under FP7. The Tier1 computing centres are supported by IN2P3 (France), KIT and BMBF (Germany), INFN (Italy), NWO and SURF (The Netherlands), PIC (Spain), GridPP (United Kingdom). We are thankful for the computing resources put at our disposal by Yandex LLC (Russia), as well as to the communities behind the multiple open source software packages that we depend on.

References

[1] M. Raidal *et al.*, *Flavour physics of leptons and dipole moments*, Eur. Phys. J. **C57** (2008) 13, `arXiv:0801.1826`.

[2] A. Ilakovac, A. Pilaftsis, and L. Popov, *Charged lepton flavor violation in supersymmetric low-scale seesaw models*, Phys. Rev. D **87** (2013) 053014.

[3] W. J. Marciano, T. Mori, and J. M. Roney, *Charged lepton flavour violation experiments*, Ann. Rev. Nucl. Part. Sci **58** (2008) 315.

[4] Heavy Flavor Averaging Group, Y. Amhis *et al.*, *Averages of b-hadron, c-hadron, and tau-lepton properties as of early 2012*, `arXiv:1207.1158`.

[5] LHCb, A. Alves *et al.*, *The LHCb detector at the LHC*, JINST **3** (2008) S08005.

[6] LHCb collaboration, R. Aaij *et al.*, *Measurement of J/ψ production in pp collisions at $\sqrt{s}$ = 7 TeV*, Eur. Phys. J. **C71** (2011) 1645, `arXiv:1103.0423`.

[7] LHCb collaboration, R. Aaij *et al.*, *Prompt charm production in pp collisions at $\sqrt{s}$ = 7 TeV*, Nucl. Phys. **B871** (2013) 1, `arXiv:1302.2864`.

[8] Particle Data Group, J. Beringer *et al.*, *Review of particle physics*, Phys. Rev. **D86** (2012) 010001.

[9] Belle collaboration, K. Hayasaka *et al.*, *Search for lepton flavor violating τ decays into three leptons with 719 million produced $\tau^+\tau^-$ pairs*, Phys. Lett. **B687** (2010) 139, `arXiv:1001.3221`.

[10] BaBar collaboration, P. del Amo Sanchez *et al.*, *Searches for the baryon- and lepton-number violating decays $B^0 \to \Lambda_c^+ \ell^-$, $B^- \to \Lambda \ell^-$, and $B^- \to \bar{\Lambda} \ell^-$*, Phys. Rev. **D83** (2011) 091101, `arXiv:1101.3830`.

[11] LHCb collaboration, R. Aaij *et al.*, *First evidence for the decay $B_s^0 \to \mu^+ \mu^-$*, Phys. Rev. Lett. **110** (2013) 021801, `arXiv:1211.2674`.

[12] A. L. Read, *Presentation of search results: the CL(s) technique*, J. Phys. **G28** (2002) 2693; T. Junk, *Confidence level computation for combining searches with small statistics*, Nucl. Instrum. Meth. **A434** (1999) 435, `arXiv:hep-ex/9902006`.

[13] R. Aaij *et al.*, *The LHCb trigger and its performance*, `arXiv:1211.3055`, to appear in JINST.

[14] T. Sjöstrand, S. Mrenna and P. Skands, *PYTHIA 6.4 Physics and manual*, JHEP **05** (2006) 026, `arXiv:hep-ph/0603175`.

[15] I. Belyaev *et al.*, *Handling of the generation of primary events in* GAUSS*, the LHCb simulation framework*, Nuclear Science Symposium Conference Record (NSS/MIC) **IEEE** (2010) 1155.

[16] D. J. Lange, *The EvtGen particle decay simulation package*, Nucl. Instrum. Meth. **A462** (2001) 152.

[17] P. Golonka and Z. Was, *PHOTOS Monte Carlo: a precision tool for QED corrections in Z and W decays*, Eur. Phys. J. **C45** (2006) 97, `arXiv:hep-ph/0506026`.

[18] GEANT4 collaboration, J. Allison *et al.*, *Geant4 developments and applications*, IEEE Trans. Nucl. Sci. **53** (2006) 270; GEANT4 collaboration, S. Agostinelli *et al.*, *GEANT4: a simulation toolkit*, Nucl. Instrum. Meth. **A506** (2003) 250.

[19] M. Clemencic *et al.*, *The LHCb simulation application, Gauss: design, evolution and experience*, J. of Phys: Conf. Ser. **331** (2011) 032023.

[20] L. Breiman, J. H. Friedman, R. A. Olshen, and C. J. Stone, *Classification and regression trees*, Wadsworth international group, Belmont, California, USA, 1984.

[21] R. E. Schapire and Y. Freund, *A decision-theoretic generalization of on-line learning and an application to boosting*, Jour. Comp. and Syst. Sc. **55** (1997) 119.

[22] A. Hoecker *et al.*, *TMVA: Toolkit for multivariate data analysis*, PoS **ACAT** (2007) 040, `arXiv:physics/0703039`.

[23] G. Punzi, *Sensitivity of searches for new signals and its optimization*, in *Statistical Problems in Particle Physics, Astrophysics, and Cosmology* (L. Lyons, R. Mount, and R. Reitmeyer, eds.), p. 79, 2003. `arXiv:physics/0308063`.

[24] J. L. Rosner and S. Stone, *Leptonic decays of charged pseudoscalar mesons*, arXiv:1201.2401.

[25] BaBar collaboration, P. del Amo Sanchez *et al.*, *Dalitz plot analysis of $D_s^+ \to K^+K^-\pi^+$*, Phys. Rev. **D83** (2011) 052001, arXiv:1011.4190.